Comparisons of methods for surface-wave noise reduction in 2D land seismic data

Jaroon Sinsawasmongkol and Chaiwoot Boonyasiriwat

ABSTRACT

In petroleum exploration, seismic primary reflections are mainly used as the signal to provide estimated images of the Earth's subsurface structures while other types of seismic events are considered as noise. In land data acquisition, the seismic data are normally corrupted with strong surface-wave noise which must be filtered out before further data processing. In this work, we implement and compare five methods for surface-wave noise reduction. The implemented methods include frequency-wavenumber filtering, seismic interferometry, radial trace transform, and local radial trace median filtering. These methods are applied to both synthetic and field seismic data. We propose to use a hybrid method which is a combination of frequency-wavenumber filtering, seismic interferometry, and local radial trace median filtering. The results show that the hybrid is more effective than each individual method.

INTRODUCTION

In 2D land seismic survey, surface waves, refracted waves, and reflected waves are recorded in the seismic data. Typically, only primary reflection events are used to image the subsurface structures while the other events including surface wave, refraction, and multiple reflections are considered as noise. The amplitude of the surface-wave noise is very strong compared to that of the primary reflection signal due to their amplitude decay nature. Therefore, in land data, surface-wave events are the main noise that must be removed to reduce strong artifacts in the estimated image of the subsurface structures.

Many surface-wave reduction methods have been proposed in the past decades. These methods include frequency-wavenumber (FK) filtering (Stewart and Schieck, 1989), radial trace transform (RTT) (Hanley, 2003), local radial trace median (LRTM) filtering (Zhu et al., 2004), polarization filtering (Shieh and Herrmann, 1990), wavelet-based filtering (Deighan and Watts, 1997), curvelet-based filtering (Yarham et al., 2009), singular value decomposition (SVD) (Chiu and Howell, 2008; Porsani et al., 2009), seismic interferometry (SI) (Halliday et al., 2007, 2010; Xue, 2010), tau-p (TP) transform (Song and Stewart, 1990), and model-driven filtering (Ke et al., 2004). FK filtering is widely used due to its simplicity and effectiveness in reducing linear noise but it typically suffers from spatial aliasing in the data. RTT and LRTM filtering can also effectively reduce linear noise but are not practical in the case of nonlinear noise. Seismic interferometry and model-driven filtering, on the other hands, can theoretically predict and reduce both linear and nonlinear noise but seismic interferometry requires a large number of data traces to obtain a prediction with a high signal-to-noise ratio (S/N), while model-driven filtering requires an accurate near-surface velocity model.

To partially overcome the drawbacks of each individual method, hybrid methods were then proposed. For examples, Hamidi et al. (2012) combined wavelet transform and singular value decomposition (SVD) techniques to reduce the low-amplitude linear surface-wave noise, and Xue (2010) used FK filtering and seismic interferometry to reduce linear surface-wave noise in the data.

In this work, we compare the effectiveness of four surface-wave noise reduction methods: FK, RTT, LRTM, TP and SI, and also compare the effectiveness of hybrid methods which are various combinations of each separate method. Both synthetic and real seismic data were used in our experiments.

METHODOLOGY

In this section, we briefly review the theory of the surface-wave noise reduction methods used in this work: FK, RTT, LRTM, TP and SI.

Frequency-wavenumber (FK) filtering can be used to reduce surface-wave noise by first transforming the seismic data from the space-time $(x-t)$ domain to the frequency-wavenumber $(f-k)$ domain using 2D Fourier transformation:

$$D(k_x,\omega) = \iint d(x,t)e^{i(k_x x-\omega t)}dxdt$$

where $d(x,t)$ represents a space-time signal, $D(k_x,\omega)$ represents a frequency-wavenumber signals, k_x represents a wavenumber in x-direction, and ω represents an angular frequency of a signal. In the $f-k$ domain, the surface-wave noise is separated from the reflection and, therefore, can be removed by muting the $f-k$ data. The $f-k$ muted data are then transformed back to the $x-t$ domain by inverse Fourier transformation:

$$d(x,t) = \iint D(k_x,\omega)e^{-i(k_x x-\omega t)}dk_\omega d\omega.$$

The effectiveness of FK filtering is reduced when the data are aliased or the surface-wave noise is discontinuous such as when the near-surface structure is complex causing scattering surface waves (Halliday et al., 2007).

Radial trace transform (RTT) can reduce the surface-wave noise in a similar way as the FK filtering in that it transforms the data from the space-time domain to the radial domain (apparent velocity-time). In the radial domain, the linear surface-wave noise appears as low-frequency components corresponding to low apparent velocities (see in Figure 1) and can be filtered out using high-pass filtering. The filtered data in the radial domain are then transformed back to the space-time domain. However, the filtering result is typically not satisfactory and need additional processing steps. Instead of filtering out the surface-wave noise in the radial domain, low-pass filtering is applied to keep only the noise which is then transformed back to the space-time domain to provide a surface-wave prediction. To remove the noise from the data, an adaptive subtraction is applied to the data using the predicted surface-wave noise.

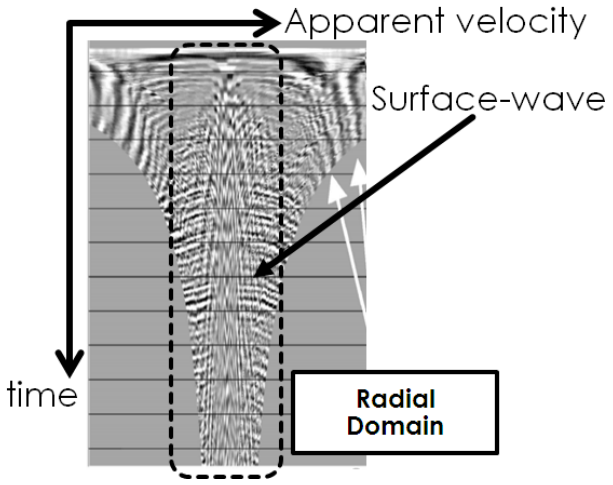

Figure 1: Surface-wave noise appears as low-frequency components in the vertical.

Local radial trace median (LRTM) filtering was proposed by Zhu et al. (2004) to eliminate the need for radial transformations. The filtering process begins by first setting a minimum and maximum apparent velocities corresponding to the surface-wave noise to be removed. This is equivalent to setting a cone-shaped region in which the surface-wave noise will be predicted. Each data sample in this region will have a single apparent velocity associated with it which corresponds to a line passing exactly through the data sample (see Figure 2). Along this line, we need to interpolate for some data samples on the left and right neighboring traces. Then, a median filter is applied to these set of data points and setting the filtering result as the surface-wave prediction at the center data point. This process is repeated for all the data samples in the cone-shaped region. Finally, adaptive subtraction is applied to remove the surface-wave noise from the data using the prediction.

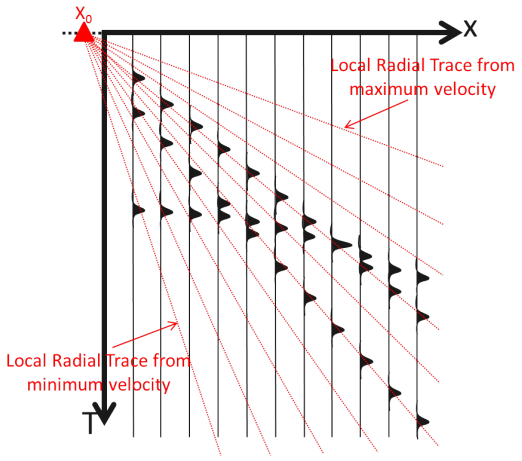

Figure 2: The cone shape of radial trace

Tau-p transform can be separated the surface-wave and the reflection. In space-time data, mostly surface-wave noise signals appeared the linear events and reflections appeared the hyperbolic events. The recorded signals can be described in term of slowness p or the reciprocal of the apparent velocity, that is a slope of linear event dt/dx in space-time domain and intercept time τ that is the arrival time obtained by projecting the slope back to zero offset point (x = 0), where x is source-receiver distance. Tau-p transform is also called slant stack, the Radon transform, and plane-wave decomposition which transforms the space-time domain data to intercept time-slowness domain data ($\tau-p$ domain data). The linear surface-wave noise transform into a point, reflection transform into ellipse. Figure 3 shows a transformation of linear and hyperbolic events in a space-time domain to tau-p domain.

Seismic interferometry (SI) can be used to predict surface-wave events in the data using cross-correlation be-

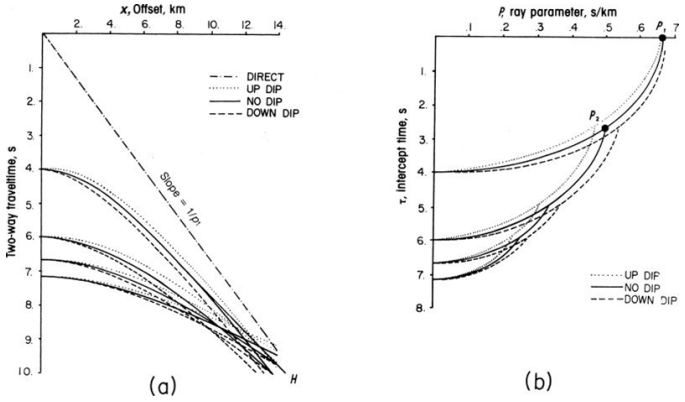

Figure 3: Tau-p (-p) mapping. (a) An seismic record signal is d(x,t) where x=source-receiver distance (offset) and t=arrival time. (b) Its tau-p transform is D(τ,p) where p=dt/dx=$1/V_a$ and τ=intercept time at x=0. Hyperbolic reflections transform into ellipses, linear events into points (the direct wave into P1, the head wave into P2). (SEG, 2012)

tween two data traces from the same source. This process is illustrated in Figure 4 in which two data traces acquired at positions A and B from the same source located at X are denoted by $d(A|X)$ and $d(B|X)$, respectively, in the time domain. Assuming the high frequency approximation and signal amplitude is negligible, the data in the frequency domain can be represented by $D(A|X) = \exp[i\omega\tau_{XA}]$ and $D(B|X) = \exp[i\omega\tau_{XB}]$ where ω is the angular frequency, τ_{XA} and τ_{XB} denote the travel times of seismic waves from X to A, and to B, respectively.

Cross-correlation is a measure of similarity of two trace signals as a function of a time-lag applied to one of them and it is defined as:

$$d(B|X,t) \otimes d(A|X,t) = \sum_{\tau=-\infty}^{\infty} d^*(B|X,\tau)d(A|X,t+\tau)$$

where $*$ denotes a complex conjugate operator, $\otimes$ denotes cross-correlation operator, and $d(B|X,t)$ and $d(A|X,t)$ represent time domain signals of $d(B|X)$ and $d(A|X)$ at time t. Cross-correlation between time domain traces is equivalent with the multiplication between two frequency domain data, given by

$$\begin{aligned} D(B|X)^* D(A|X) &= \exp[-i\omega\tau_{XB}]\exp[i\omega\tau_{XA}] \\ &= \exp[i\omega(\tau_{XA}-\tau_{XB})] \\ &= \exp[i\omega\tau_{BA}] \\ &= D(A|B) \end{aligned}$$

where $D(A|B)$ denotes the predicted surface-wave data from the virtual source B to the receiver A. In practice, the predicted surface-wave signal will be corrupted with noise and more predictions from several source locations are needed to improve the S/N of the prediction which is then used by adaptive subtraction to remove the surface-wave noise from the data.

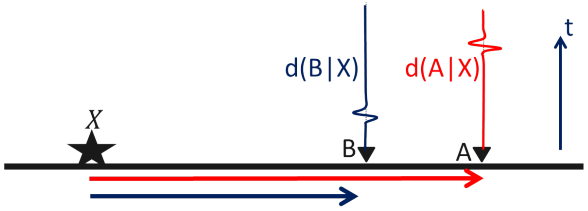

Figure 4: A surface wave travels from seismic source at X to receivers at B and A. Surface-wave signals are recorded in the time domain and represented by $d(B|X)$ and $d(A|X)$.

RESULTS AND DISCUSSION

In this section, the implemented methods are applied to a synthetic and two sets of field data to investigate the effectiveness of each method in reducing the surface-wave noise.

The synthetic data used are comprised of 3 hyperbolic and four linear events, corresponding to primary reflection signals and surface-wave noise, respectively. The linear events correspond to the apparent velocity of $\pm$1000 m/s and $\pm$2000 m/s. Figure 5a shows the synthetic data recorded by 360 channels of receivers with a receiver spacing of 50 m, a time sampling interval of 2 ms, and the total record length of 7 s. To make the synthetic data similar to the field data, the amplitude of surface-wave noise is five times that of the hyperbolic events. The reference data show in Figure 5b that do not include linear noises. We then apply all five filtering methods to the data and obtain the results to compare the effectiveness of each method. We compute the residual of the surface-wave noise defined by

$$r = \frac{\|f(d) - d_{ref}\|}{\|d_{ref}\|} \times 100$$

where r is the residual, $f(d)$ is the filtering result, and d_{ref} is reference data.

Figure 6a and 6b show the synthetic data and FK filtering result in fk domain. The FK result shows the reduction and the residual linear events. The residual linear event due to the aliasing signals and can be transformed back to the residual linear noise in FK result that shows in Figure 10a. Figure 7a shows the synthetic data in radial domain that include low-frequency signals of linear noise and hyperbolic events of reflection. Low-frequency filtering result in Figure 10b shows the reduction of hyperbolas and residual low-frequency signals that correspond to the predicted linear noise in Figure 8a.

Figure 8 shows the linear noise prediction of synthetic data and show noise prediction effectiveness of RTT,LRTM, and SI. RTT and LRTM prediction in Figure 8a and b correspond with linear noises in synthetic data but SI prediction in Figure 8 do not correspond. From Figures 9a and 9b show SI testing data that include four linear noise

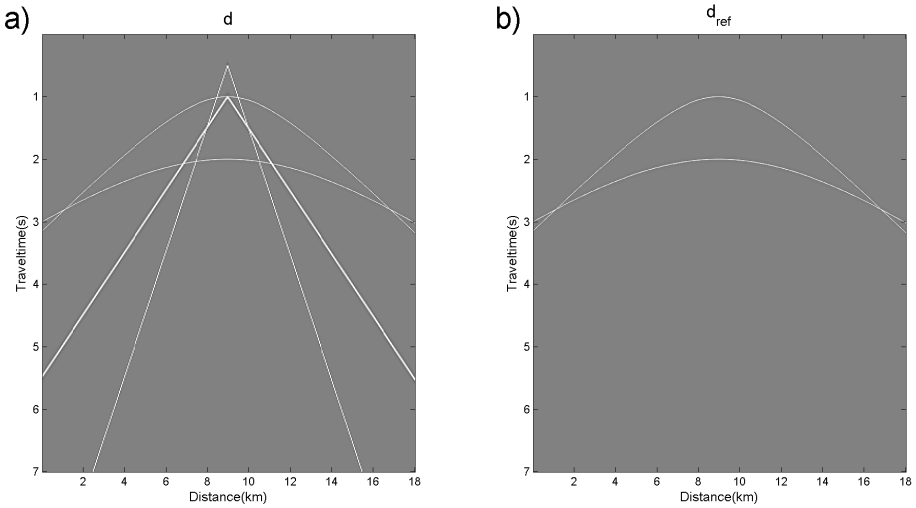

Figure 5: The hyperbolic events as primary reflection events and linear events as surface-wave noises. a) the synthetic data (d) include two hyperbolic events and four linear noises. b) the reference data (d_{ref}) include two hyperbolic events.

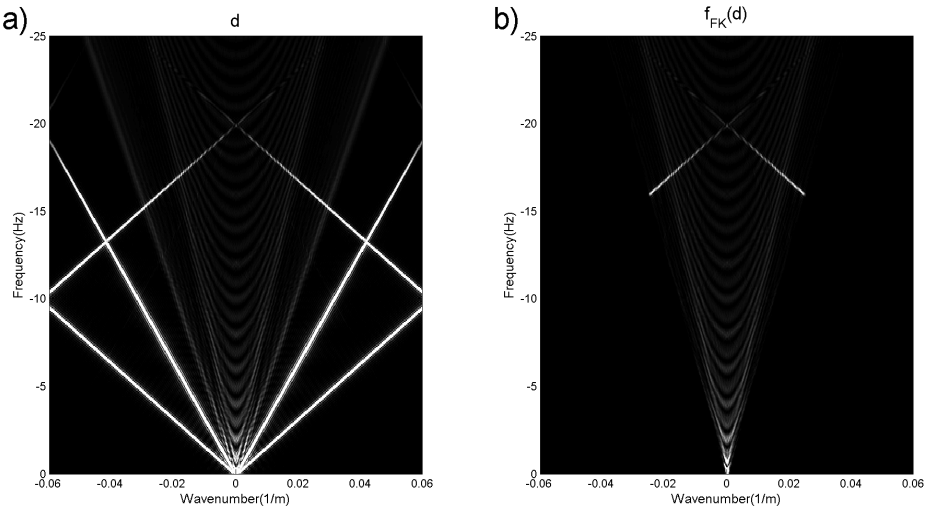

Figure 6: The linear noises transform to linear events in fk domain. a) The synthetic data (d) in fk domain include linear noise signals. b) FK filtering result ($f_{FK}(d)$) in fk domain show the reduction and residual of linear noises.

where their zero offsets are a source position and the SI prediction of the testing data. SI has high effectiveness to detects the linear noise where their zero offsets are a source point.

The implemented method results in Figure 10a-c are FK, RTT, and LRTM results that include residual hyperbolas and very low-amplitude of linear noises. The amplitudes of near-offset hyperbolas in RTT result are reduced therefore RTT is less refleced conservation than FK and LRTM. LRTM result shows stronger residual near-offset linear noises therefore the linear reduction effectiveness of LRTM is less than FK and RTT. The resitduals of the filtering results using FK, RTT, LRTM ,and SI are 35.11%, 84.14%, 69.20%, and 88.25% that correspond with their effectiveness. SI result has very low effectiveness compare to FK, RTT, and LRTM because it can not predict linear noise where their zero offsets are not a source.

First field data set used in second experiment are compried of reflections and linear surface-wave noise. The linear surface-wave amplitudes are not stronger than reflections that show in Figure 11. This field data set recorded ny 360 channels with a receiver spacing of 50 m, a time sampling interval of 2 ms, and total record length of 7 s. In this experiment, we interested in 4 s of recorded data.

Figure 12a and b are the field data and FK result in fk domain that show the reduction of surface-wave signals in low-slope regions. The surface-wave predictions of RTT and SI show in Figure 13a - b. RTT prediction includes the linear events of surface-wave but SI does not include. Because surface-wave in the field data do not strong, the

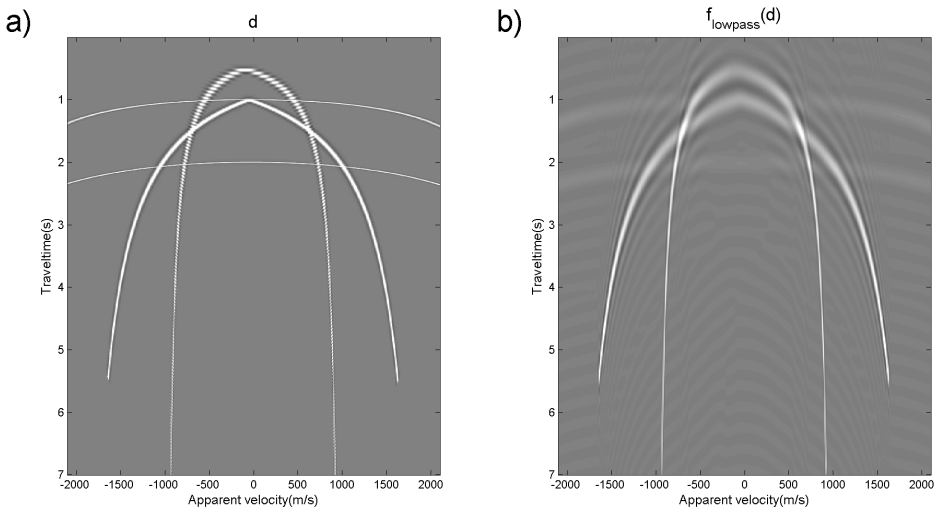

Figure 7: The linear noises transform to low-frequency signals in vertical componet. a) The synthetic data (d) in radial domain include the hyperbolic events of reflection and low-frequency signals of linear noise. b) The lowpass filtering result of synthetic data ($f_{lowpass}(d)$) in radial domain shows low-frequency signal of linear noise and residual hyperbolic signals.

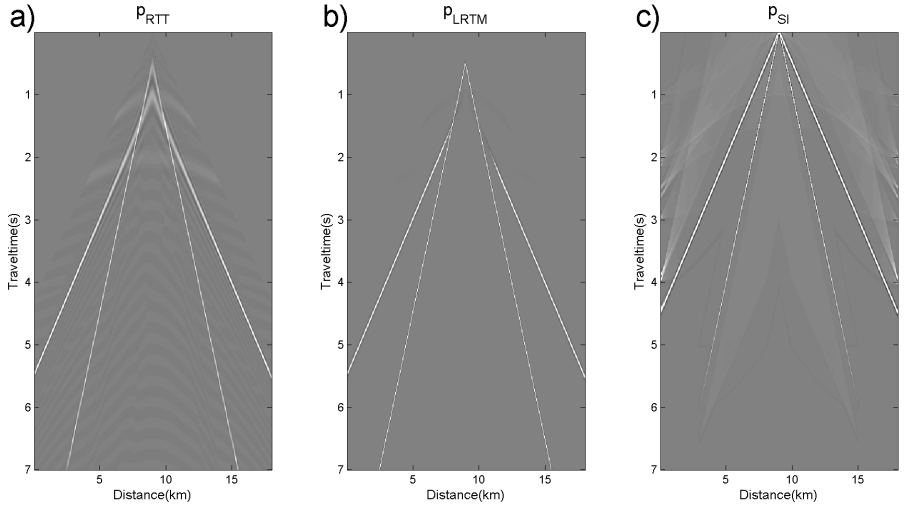

Figure 8: The linear events due to the linear noise prediction from the implemented methods: a) RTT, b) LRTM, and c)SI

stacking signals of SI surface-wave prediction are not different from their artifacts.

The surface-wave reducing effectiveness can be discuss from Figure 14a-c that are FK, RTT, and SI results. The linear surface-waves in FK and RTT results are reduced with more efficiency than SI but the signals on near-offset traces in FK result do not clear. SI result shows the reduction in low-effectiveness that is affected of the comfusion in its prediction.

The hybrid method that is a combition of the implemented methods is designed to improve the surface-wave filtering effectiveness. In this field data set, The hybrid method is a combination of RTT and FK. RTT method is applied in the first of a workflow to reduce surface-wave noise. The residual of surface-waves are included with very low amplitudes on far-offset traces but with medium amplitude on near-offset traces that show in Figure 15b. The hybrid result (the combinated result of FK and RTT) in Figure 15c shows the reduction of residual surface-wave on near-offset traces and its reflections are more clearly compared to the field data and RTT result in Figure 15a-b.

The field data set 1 used in the second experiment are comprised of reflections and linear surface-wave events. The linear surface-wave noise is very strong compared to the reflections and can be separated into two groups:

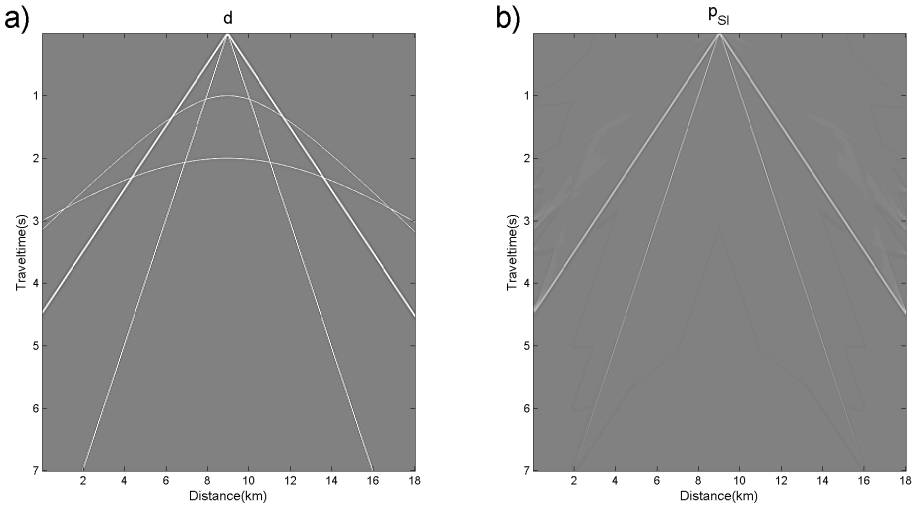

Figure 9: a) The SI testing data and b) its SI prediction

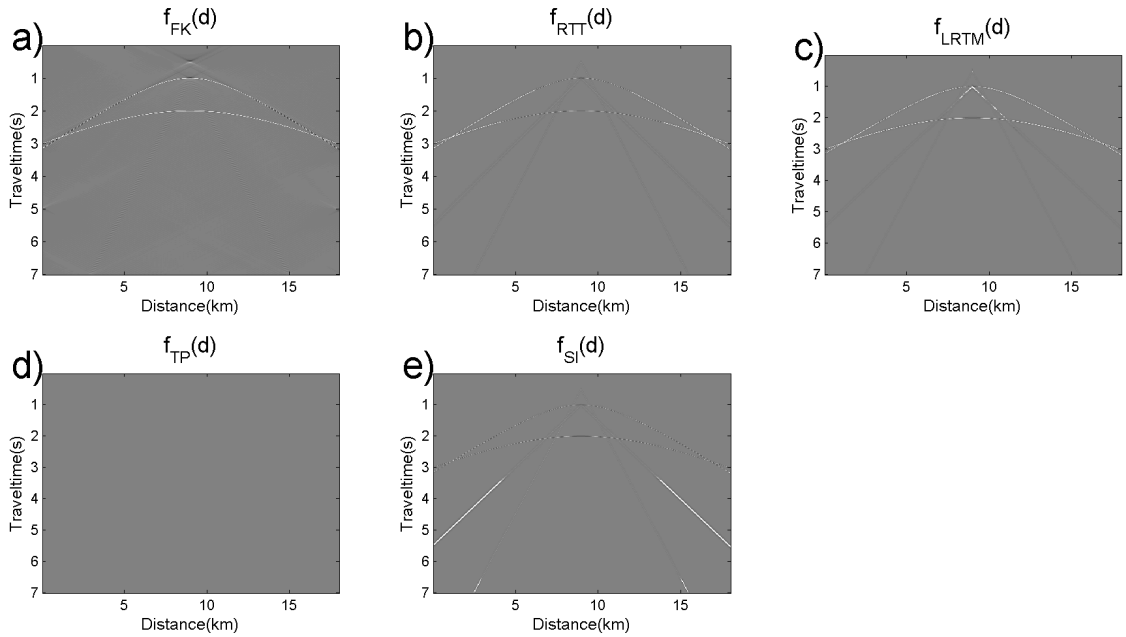

Figure 10: The results of implemented method: a) FK, b) RTT, c) LRTM, d) TP, and e) SI.

mildly and steeply dipping events shown in Figure 16a. The field data were recorded by 240 channels of receivers with a receiver spacing of 30 m, a time sampling interval of 4 ms, and total record length of 2 s. We then apply all implemented filtering methods to the data and obtain the results shown in

The residual of surface-wave noise using FK shows in Figure 16b that include the residual mildly events but the dipping events are removed. Both the residual mildly surface-wave and the residual dipping surface-wave noise amplitudes of SI and RTT (Figure 16c-d) are reduced compared to the data but the reductions are low effectiveness compared to FK filtering. The LRTM result shows in Figure 16f and it has not the residual surface-wave noise. The LRTM result includes the artifacts that can destroy the primary reflection in surface-wave regions with moderately amplitude compared to the primary reflection. After the filtering comparison, the hybrid method designed by the combination of three filtering methods: FK, SI, and LRTM. FK filtering is applied to the data in the first of a workflow to remove dipping surface-wave and apply SI in the second to reduce mildly dipping surface-waves. The residual surface-waves after FK and SI are reduced by LRTM. LRTM used on only the residual surface-wave regions to reduce their artifact amplitude and control the artifact regions. Hybrid result shows in Figure 16f that

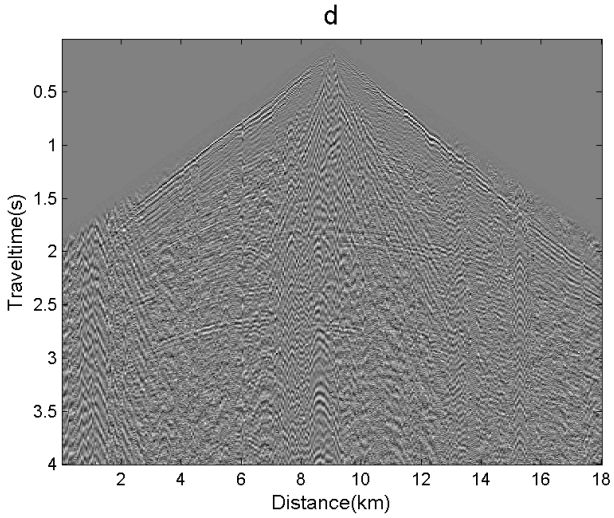

Figure 11: The example of first field data (d) set shows the linear surface-wave noise.

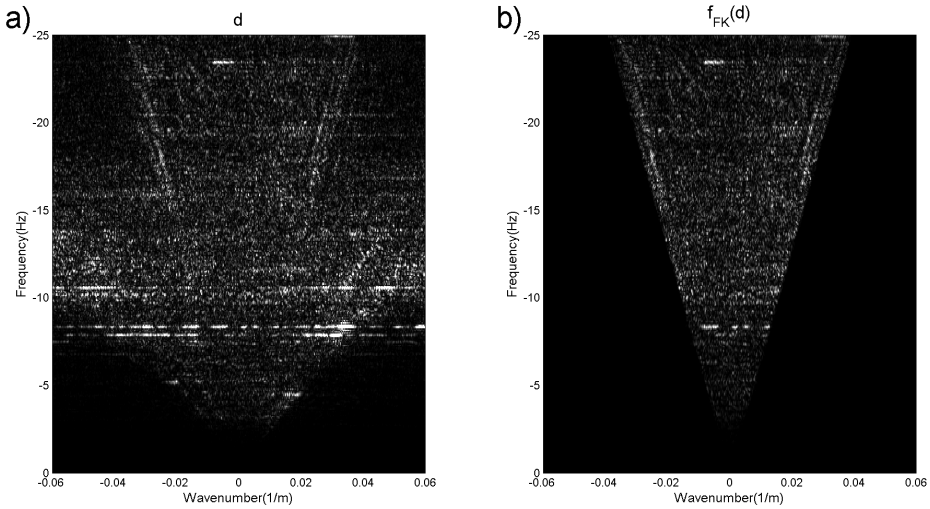

Figure 12: a) The seismic signals in fk domain are very confused. Moreever, surface-wave do not completely seperate from the reflections. b) The residual signals in muted result correspond the reflection signals.

shows higher effectiveness of the reduction compared to the individual implemented results.

The difference of field data used in the third experiment. They include the non-linear events of surface-wave noise in stronger amplitude compared to the primary reflection. Figure 17a shows the field data recorded by same parameters of second experiment data. We then apply all four filtering methods to the data and obtain the results. To compare the separated methods, we compute the amplitude of residual non-linear surface-wave and residual primary reflection compared to the data (Figure 17a). The residuals of surface-wave noise using the individual filtering show in Figure 17b-e that have lower reduction effectiveness compared to the effectiveness of the linear noise reduction in second experiment. The surface-wave noise after FK and LRTM (Figure 17b and 17e) are more reduced than SI and RTT (Figure 17c and 17d). Both SI and RTT show the very low effectiveness of the non-linear reduction because the amplitude of the noise in their results as same as the data in Figure 17a. The hybrid result shown in Figure 17f that include the lower surface-wave and the more reflection amplitudes compared to the individual filtering results.

SUMMARY

We have implemented the methods for reducing surface-wave noise: FK filtering, radial trace transform, local radial trace median filtering, and seismic interferometry.

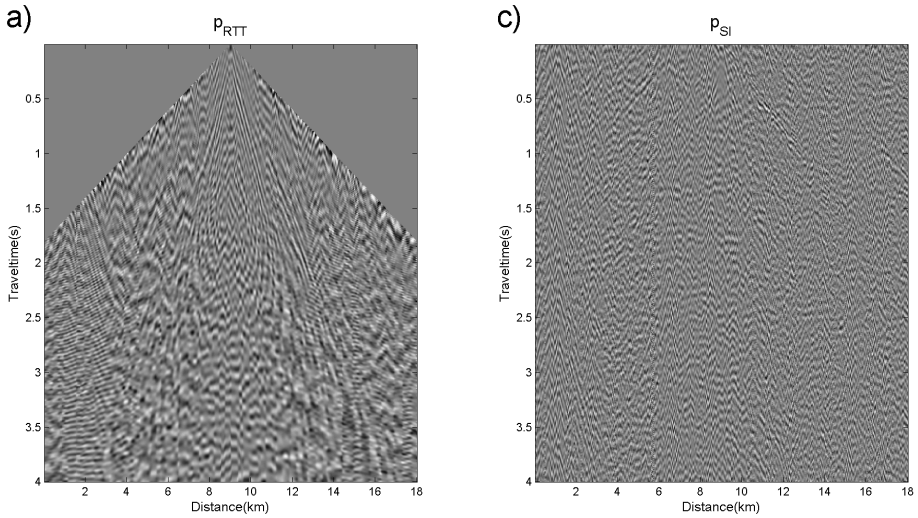

Figure 13: The surface-wave prediction of the implemented methods: a) FK, b) RTT, and c) SI.

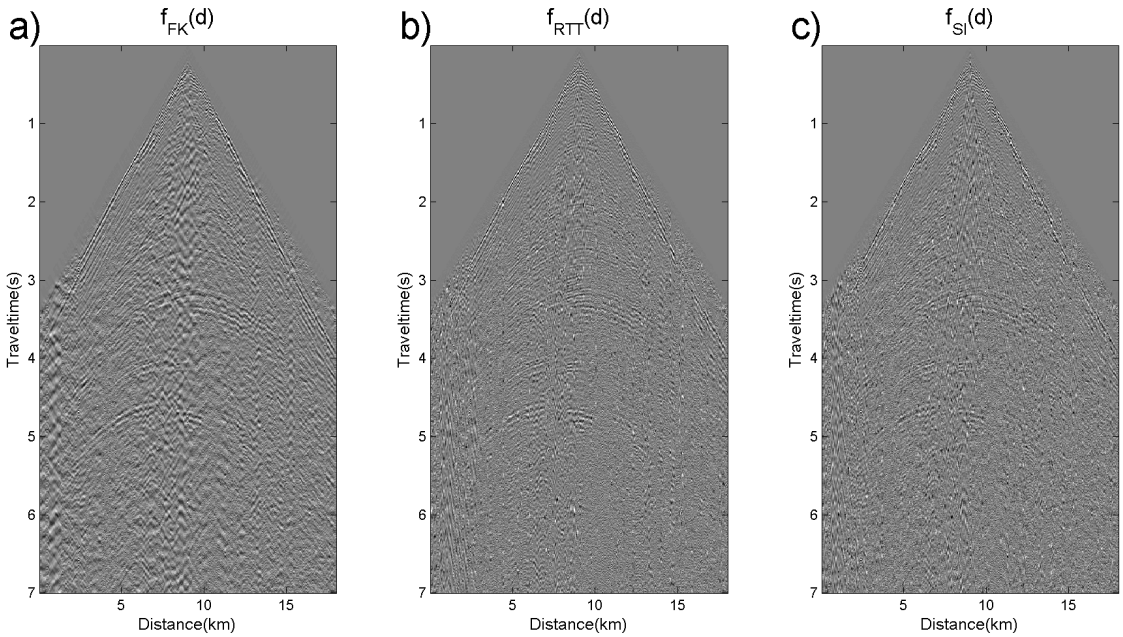

Figure 14: The results of implemented filtering methods: a) FK, b) RTT, and c) SI.

ACKNOWLEDGMENTS

We are grateful to the support from PTTEP and would like to thank Thailand Research Fund for partially supporting this research under the contract MRG5480280.

REFERENCES

Chiu, S. K. and J. E. Howell, 2008, Attenuation of coherent noise using localized-adaptive eigenimage filter: SEG Expanded Abstracts, 2541–2544.

Deighan, A. J. and D. R. Watts, 1997, Ground-roll suppression using the wavelet transform: Geophysics, **62**, 1896–1903.

Halliday, D., A. Curtis, J. A. Robertsson, and D. V. Manen, 2007, Interferometric surface-wave isolation and removal: Geophysics, **72**, A69–A73.

Halliday, D., A. Curtis, P. Vermeer, C. Strobbia, A. Glushchenko, D. V. Manen, and J. A. Robertsson, 2010, Interferometric ground-roll removal: Attenuation of scattered surface waves in single-sensor data: Geophysics, **75**, SA15–SA25.

Hamidi, R., A. Javaherian, and A. M. Reza, 2012, Ground roll attenuation based on a hybrid wavelet transform and singular value decomposition: SEG Expanded Abstracts.

Hanley, D. V., 2003, Coherent noise attenuation in the

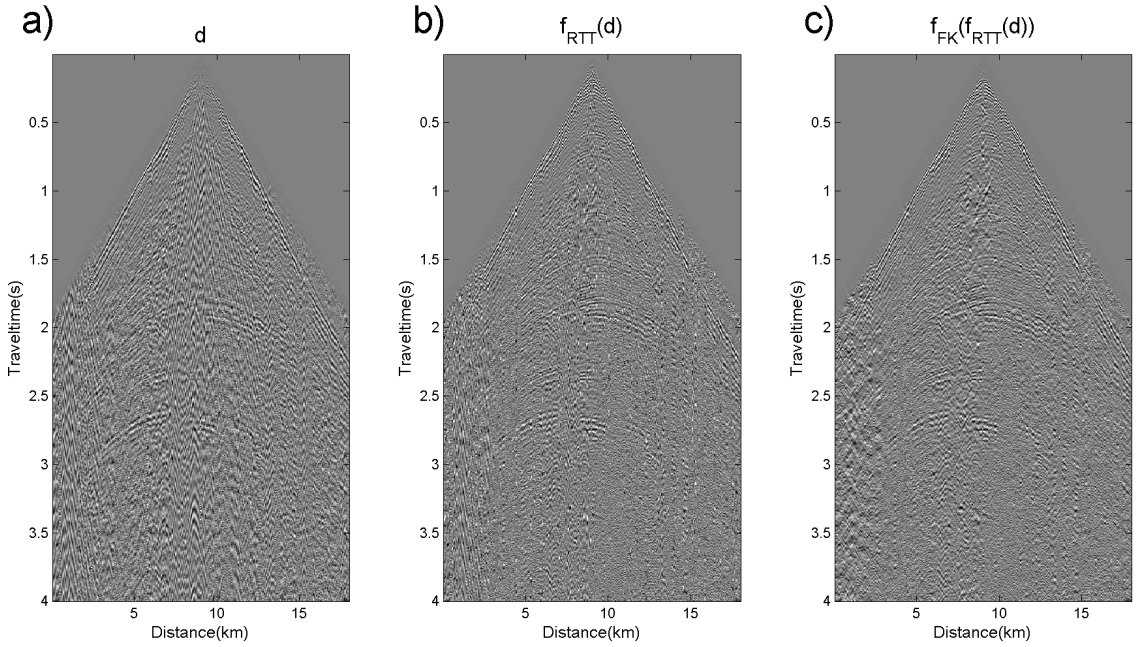

Figure 15: The comparison of a) field data, b) RTT result, and c)hybrid result shows the reducing of surface-wave and conservation of reflections.

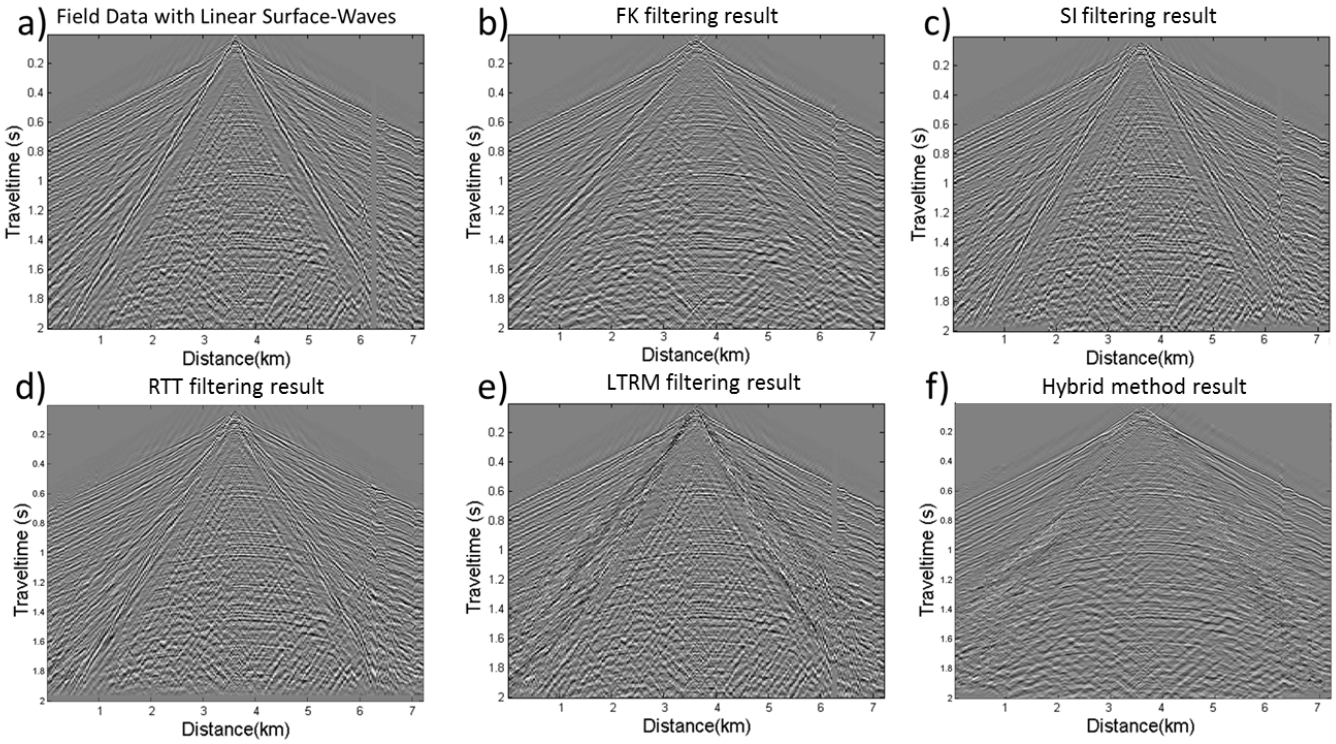

Figure 16: Field data (with linear surface-waves) results: (a) field data, and filtered data after (b) f-k filtering, (c) seismic interferometry filtering, (d) radial trace transform filtering, and (e) local radial trace median filtering, and (f) hybrid filtering.

radial trace domain: Geophysics, **68**, 1408–1416.

Ke, B., B. Zhao, C. Liu, and W. Geng, 2004, Model-driven filtering based on wave propagation features: SEG Expanded Abstracts, 2128–2131.

Porsani, M. J., M. G. Silva, P. E. M. Melo, and B. Ursin, 2009, Ground-roll attenuation based on SVD filtering:

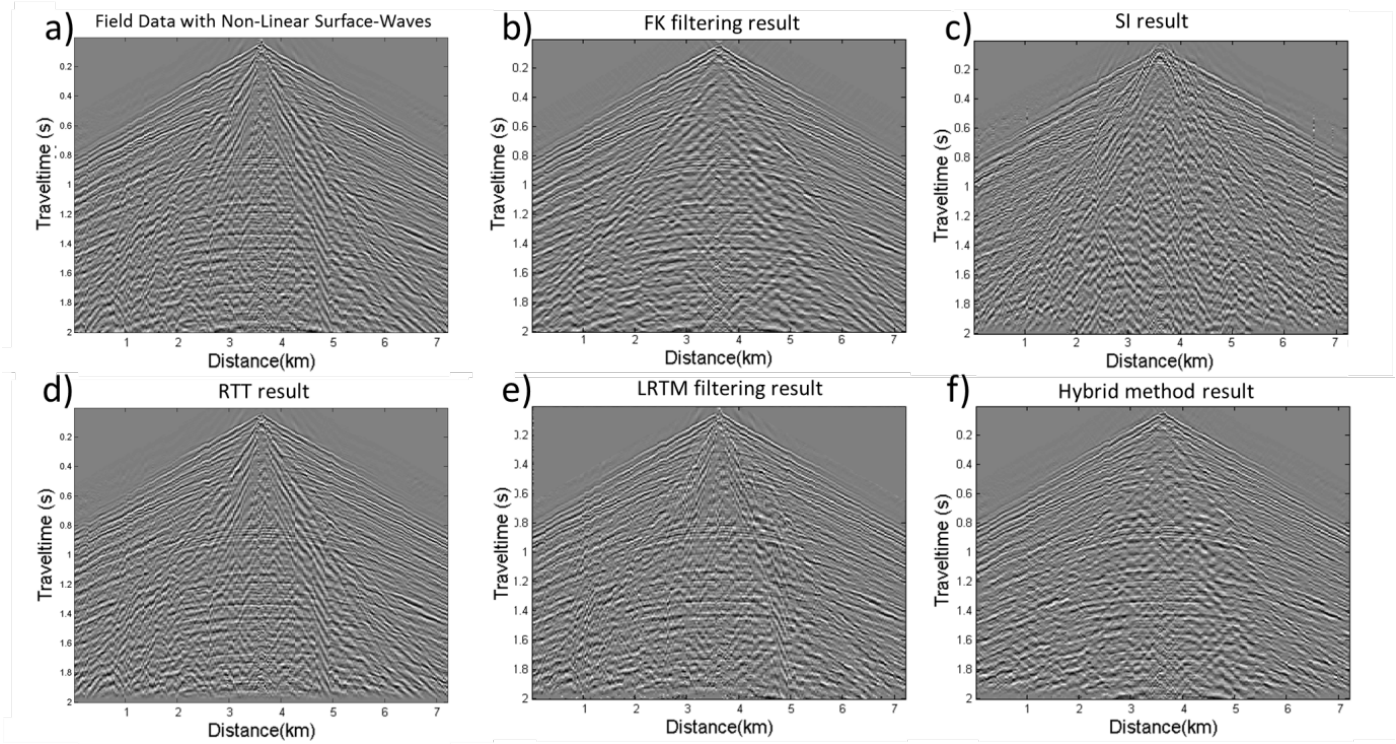

Figure 17: Field data (with non-linear surface-waves) results: (a) field data, and filtered data after (b) f-k filtering, (c) seismic interferometry filtering, (d) radial trace transform filtering, and (e) local radial trace median filtering, and (f) hybrid filtering.

SEG Expanded Abstracts, 3381–3385.

SEG, 2012, tau-p mapping (τ-p).

Shieh, C.-F. and R. B. Herrmann, 1990, Ground roll: Rejection using polarization filters: Geophysics, **55**, 216–1222.

Song, Y. and R. R. Stewart, 1990, Ground roll rejection via F-V filtering: SEG Expaned Abstracts, 1322–1325.

Stewart, R. R. and D. G. Schieck, 1989, 3-D F-K filtering: SEG Expanded Abstracts, 1123–1124.

Xue, Y., 2010, Least squares datuming and surface waves prediction with interferometry: PhD thesis, University of Utah.

Yarham, C., U. Boeniger, and F. Herrmann, 2009, Curvelet-based ground roll removal: SEG Expanded Abstracts, 2777–2782.

Zhu, W., P. G. Kelamis, and Q. Q. Liu, 2004, Linear noise attenuation using local radial trace median filtering: Leading Edge, **24**, 728–731.